



HAL
open science

Ab Initio Screening of Divalent Cations for CH₄, CO₂, H₂, and N₂ Separations in Chabazite Zeolite

Ayoub Daouli, Jérôme Rey, El Hassane Lahrar, Valentin Valtchev, Michael Badawi, Rémy Guillet-Nicolas

► **To cite this version:**

Ayoub Daouli, Jérôme Rey, El Hassane Lahrar, Valentin Valtchev, Michael Badawi, et al.. Ab Initio Screening of Divalent Cations for CH₄, CO₂, H₂, and N₂ Separations in Chabazite Zeolite. *Langmuir*, 2023, 39 (45), pp.15962-15973. 10.1021/acs.langmuir.3c01882 . hal-04295506

HAL Id: hal-04295506

<https://hal.science/hal-04295506>

Submitted on 20 Nov 2023

HAL is a multi-disciplinary open access archive for the deposit and dissemination of scientific research documents, whether they are published or not. The documents may come from teaching and research institutions in France or abroad, or from public or private research centers.

L'archive ouverte pluridisciplinaire **HAL**, est destinée au dépôt et à la diffusion de documents scientifiques de niveau recherche, publiés ou non, émanant des établissements d'enseignement et de recherche français ou étrangers, des laboratoires publics ou privés.

***Ab initio* screening of divalent cations for CH₄, CO₂, H₂ and N₂ separations in chabazite zeolite**

Ayoub Daouli,^{a†} Jérôme Rey,^{a,b†*} El Hassane Lahrar,^b Valentin Valtchev,^b Michael Badawi,^{a*}
Rémy Guillet-Nicolas,^{b*}

^a *Laboratoire de Physique et Chimie Théoriques, CNRS, Université de Lorraine, 54506 Vandœuvre-lès-Nancy, France.*

^b *Normandie Université, ENSICAEN, UNICAEN, CNRS, Laboratoire Catalyse et Spectrochimie, 14000, Caen, France.*

[†]: A.D. and J.R. contributed equally to this work.

*Emails: michael.badawi@univ-lorraine.fr; remy.guillet@ensicaen.fr

Abstract

The efficient separation and adsorption of critical gases is, more than ever, a major focus point in important energy processes, such as CH₄ enrichment of biogas or natural gas, CO₂ separation and capture, and H₂ purification and storage. Thanks to its physicochemical properties, cation exchanged chabazite is a potent zeolite for such applications. Previous computational screening investigations have mostly examined chabazites exchanged with monovalent cations. Therefore, in this contribution, periodic density functional theory (DFT) calculations in combination with dispersion corrections have been used for a systematic screening of divalent cation exchanged chabazite zeolites. The work focuses on cheap and readily available divalent cations, Ca(II), Mg(II), and Zn(II), Fe(II), Sn(II) and Cu(II) and investigates the effect of the cation nature and location within the framework on the adsorption selectivity of chabazite for specific gas separations, namely CO₂/CH₄, N₂/CH₄, and N₂/H₂. All the cationic adsorption sites were explored to describe the diversity of sites in a typical experimental chabazite with a Si/Al ratio close to 2 or 3. The results revealed that Mg-

CHA is the most promising cation for the selective adsorption of CO₂. These predictions were further supported by *ab initio* molecular dynamics simulations performed at 300 K which demonstrated that the presence of CH₄ has a negligible impact on the adsorption of CO₂ on Mg-CHA. Ca(II) was found to be the most favorable cation for selective adsorption of H₂ and CO₂. Finally, none of the investigated cations were suitable for preferential capture of N₂ and H₂ in the purification of CH₄ rich mixtures. These findings provide valuable insights into the factors influencing the adsorption behavior of N₂, H₂, CH₄, and CO₂ and highlight the crucial role played by theoretical calculations and simulations for the optimal design of efficient adsorbents.

Keywords : separation, adsorption, zeolite, chabazite, DFT, biogas, hydrogen, energy.

Introduction

Separation technology is a critical aspect of several major industries, including petrochemicals, mining, nuclear and electronics. In the ongoing energy transition, separation processes are heavily correlated with lower energy consumption, improved efficiency, selectivity, and greater sustainability. For example, the direct capture and sequestration of carbon dioxide (CO₂) being present in low concentrations (< 400 ppm)¹ from air is currently being intensively investigated to mitigate anthropogenic greenhouse gas emissions. To achieve this objective, it is essential to selectively adsorb CO₂ in comparison to other gases such as diazote (N₂). CO₂ is a significant impurity in natural gas, biogas, and flue gas, with concentration ranging between 3-20%,^{2,3} making selective adsorption of CO₂ critical. Similarly, diazote is an inevitable impurity in bio- or natural gas, limiting the heating value of the methane (CH₄). Thus the selective separation of CO₂/CH₄ and N₂/CH₄ is crucial in methane enrichment.⁴ Finally, with the increasing interest in dihydrogen (H₂) as the next generation clean energy carrier, its efficient purification and storage is a key challenge that

presently limits its utilization and democratization.⁵ At present, H₂ is primarily produced by steam methane reforming, implying effective separation from major impurities, namely CO₂, CH₄ and N₂ to enhance its usability and added value.

Despite the considerable progress in meeting diverse separation requirements with "traditional" techniques such as distillation and extraction, the associated energy consumption, particularly for cryogenic distillation, remains exorbitant, accounting for 10-15% of the world's total energy consumption.⁶ Therefore, the need to identify economical and sustainable separation technologies is imperative to reduce the overall energy consumption and environmental emissions. In this way, adsorption-based methods appear highly desirable alternatives,³ relying heavily on performant nanoporous materials. Several promising candidates for this purpose have emerged over the last decades, with zeolites being of considerable interest. Zeolites are crystalline microporous aluminosilicates that are ubiquitous in many commercial applications, including the adsorption, separation, and storage of gases,⁷ as well as catalytic applications such as hydrocarbons transformation⁸ and biomass conversion.⁹ Zeolites exhibit properties such as stability, non-toxicity and non-corrosiveness, low cost, fast kinetics of adsorption, and low energy requirement for regeneration.¹ Zeolites are also extremely stable to thermal and hydrothermal treatments.^{10,11} Zeolites have been utilized in separation processes for more than two centuries and continue to be the foremost candidates for material-based separations.

Currently, more than 250 different zeolitic frameworks are known.¹² This vast diversity of structures is responsible for a wide range of chemical properties related to shape-selectivity. Zeolites can be classified according to their main pore dimensions, with small (3.0–4.5 Å), medium (4.5–6 Å), large (6.0–8.0 Å), and extra-large (>8.0 Å) pore zeolites. Among these, small pore zeolites (with pores accessible through small 8-membered ring windows, i.e., windows delimited by 8 tetrahedral atoms, Si or Al) are highly suitable for upgrading small-

molecule feedstocks.¹³ Here we selected chabazite (CHA), a small pore zeolite with numerous applications,¹² owing to its exceptional performance in cation exchange, desiccation¹⁴, adsorption or separation as a molecular sieve,³ and catalysis. For instance copper exchanged chabazite (Cu-SSZ-13) is employed for the depollution of diesel engines via the Selective Catalytic Reduction of nitrogen oxides¹⁵ or in the methanol-to-olefin (MTO) process¹⁶, along with SAPO-34, a silico-alumino-phosphate with the chabazite topology.

In this work, we focused on the selective adsorption of small molecules from biogas, namely, methane CH₄, carbon dioxide CO₂, dinitrogen N₂ and dihydrogen H₂. These small molecules have kinetic diameters of 3.76, 3.3, 3.64 and 2.69 Å,^{3,17} respectively, and can access the cavities of chabazite via the small eight-membered rings pores of approximate dimension of 3.8 × 3.8 Å.¹² Chabazite is therefore an excellent candidate for these gas molecules adsorptions. Indeed, Zhang et al. have found that chabazites exchanged with alkali and alkaline earth cations exhibit good adsorption selectivity for CO₂/N₂ mixtures,¹⁸ and that Zn-CHA has a high capacity for adsorption of CO₂ at low concentrations.¹ Ramos et al.^{19,20} have investigated the adsorption of CO₂, CH₄ and N₂ adsorption in cation-exchanged silico-alumino-phosphates SAPO-34 (same framework as chabazite) and have shown a moderate selectivity toward CH₄/N₂ mixtures and a good separation of CO₂ with other gas with the presence of strontium cation. A particular phenomenon that affects the selectivity in chabazite, is the molecular trapdoor effect that produces a counter-intuitive size inverse sieving.²¹⁻²³ This effect consists of the displacement of "door keeping" extra-framework cations located at the center of 8-membered ring windows by molecules in strong interaction with them. This phenomenon allows these molecules to selectively enter the cavities while molecules with weak extra-framework cation interactions cannot, ultimately resulting in a high selectivity in chabazite.²⁴ It is important to note that the gating is temperature dependent and working below a certain critical temperature is mandatory to observe it. For instance, one

must be below 293 K for N₂ and CH₄ separations in K-CHA.²² During the last years, different theoretical studies on molecule interactions in zeolites were carried out, such as methane and nitrogen interactions with alkali and alkaline earth cations within zeolites.²⁵⁻²⁷ However, most of the studies in the literature so far deal with monovalent cations exchanged zeolites only, investigating divalent cations is important, especially considering the potential of inexpensive and easily available metal divalent ones (e.g., Mg²⁺, Ca²⁺, Fe²⁺, Cu²⁺, Zn²⁺ and Sn²⁺). Our objective is thus to identify the most promising divalent cations suitable for biogas and dihydrogen purification that could meet the technical and economical requirements of present and future energy-related separation processes.

To save time and resources in experimental (post-)synthesis work that is still, unfortunately, mostly based on trial and errors approaches, Density Functional Theory (DFT) calculations are useful to understand, compare and predict with a good accuracy adsorption properties of zeolites.^{15,28} The advantage of combining simulations and experiments to identify optimized materials for adsorption processes have been demonstrated in previous works.²⁹⁻³² For example, DFT cation screenings were performed in faujasite to investigate CO₂ adsorption,³³ selective removals of NO_x and CO from diesel gas exhaust^{34,35} or for CO₂/N₂ separation.²⁹ H₂S selective adsorption was studied in Y zeolite³⁶ and iodine species capture in faujasite²⁸ or mordenite.³⁷

In this line, in the first part of this computational study, we systematically investigated the relative stabilities of the possible locations of divalent extra-framework cations in the chabazite framework, taking into account the different possible distributions of aluminium atoms. In the second part, adsorption energies of CO₂, CH₄, N₂ and H₂ over these divalent cation-exchanged chabazite were computed to identify the best divalent cations for the separations of different binary mixtures containing CO₂, CH₄, N₂ and H₂, being of utmost current interest in both academia in industry. Finally, *ab initio* molecular dynamics (AIMD)

was used to probe the co-adsorption of CH₄ and CO₂ molecules at a finite temperature of 300 K on the most promising divalent cation identified for the CO₂ / CH₄ separation, providing valuable insights into the potential of divalent cation exchanged CHA zeolite for purification of bio- and natural gas.

Materials and Methods

Structural and computational details

Structural Model

Chabazite is a small pore zeolite³⁸ with a three-dimensional network consisting of stacked sequences of 6-membered rings, resulting in hexagonal prisms (or double-six rings, D6R) linked together by four-membered rings (4MRs). The resulting framework contains relatively large ellipsoidal cavities of $6.7 \times 10 \text{ \AA}$. Each cavity can be accessed by six eight-membered rings (8MR) windows that have an approximate dimension of $3.8 \times 3.8 \text{ \AA}$.¹² In our simulations, we used a chabazite supercell of 72 atoms (24 Si and 48 O), as in previous work.³⁹ This supercell is large enough to avoid any artificial interactions between molecules and their periodic images, with distances greater than 7 \AA . This triclinic cell is defined by the following lattice parameters: $a = 12.712 \text{ \AA}$, $b = 13.711 \text{ \AA}$, $c = 9.365 \text{ \AA}$, $\alpha = 90.32^\circ$, $\beta = 96.82^\circ$,

$\gamma = 89.93^\circ$, resulting in a cell volume of 1620.6 \AA^3 (

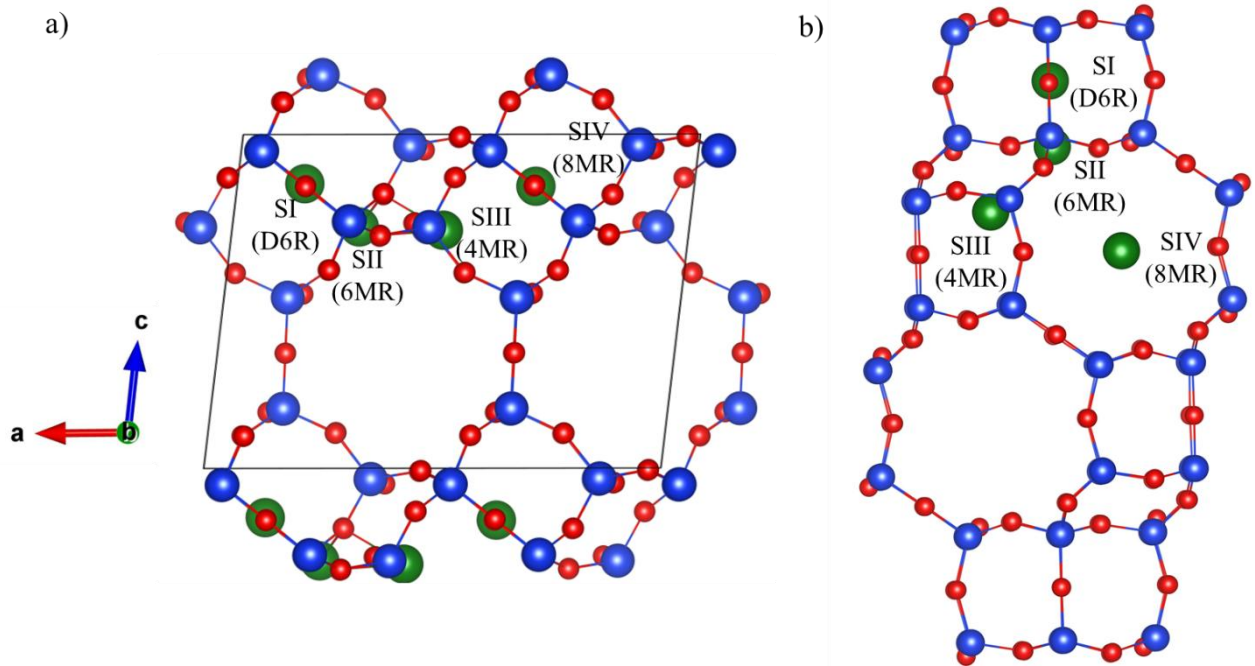


Figure 1.a).

The substitution of two silicon tetrahedra SiO_4 with two aluminum tetrahedra AlO_4^- in the chabazite zeolite structure generates two negatively charged AlO_4^- in the framework and the electroneutrality is compensated by the incorporation of an extra-framework divalent cation (

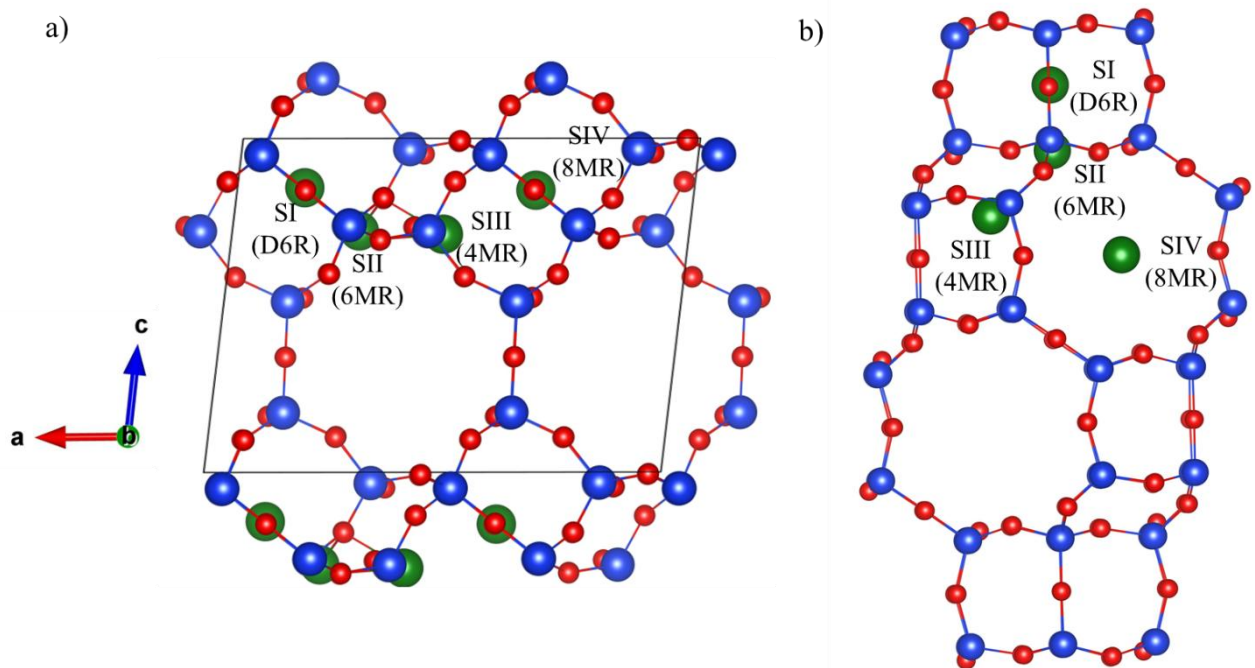


Figure 1.b), resulting in a Si/Al ratio of 11. Therefore, the molecular formula of the studied cell is $M_1Al_2Si_{22}O_{48}$ with $M = Ca^{2+}, Mg^{2+}, Fe^{2+}, Cu^{2+}, Zn^{2+},$ or Sn^{2+} .

The structural studies of ion-exchanged chabazite reveals four type of extra-framework cationic sites:^{23,40-44}: i) at the center of D6R prism (SI), ii) in the large cavity near the 6MR (SII), iii) in the large cavity near the 4MR opening of a D6R prim (SIII) and iv) in the center of the 8MR window of the large cavity , denoted SIII^{41,42} or SIV⁴⁰ in the literature (we will use SIV in this work). These sites are shown in

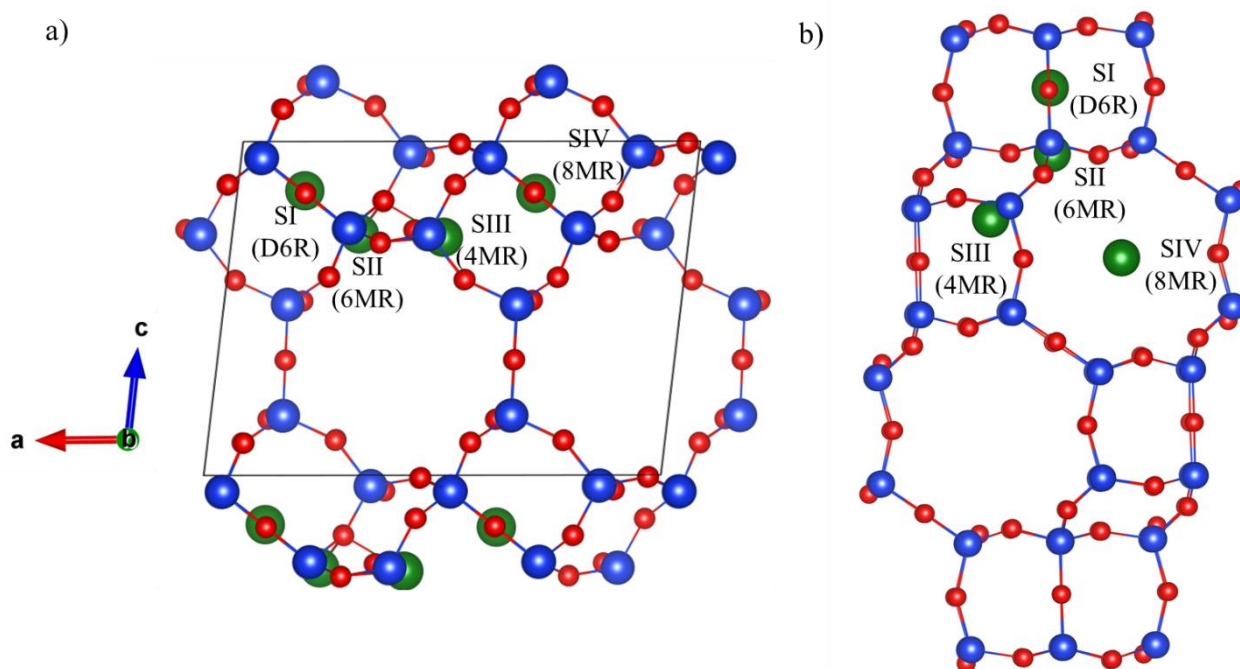


Figure 1.b.

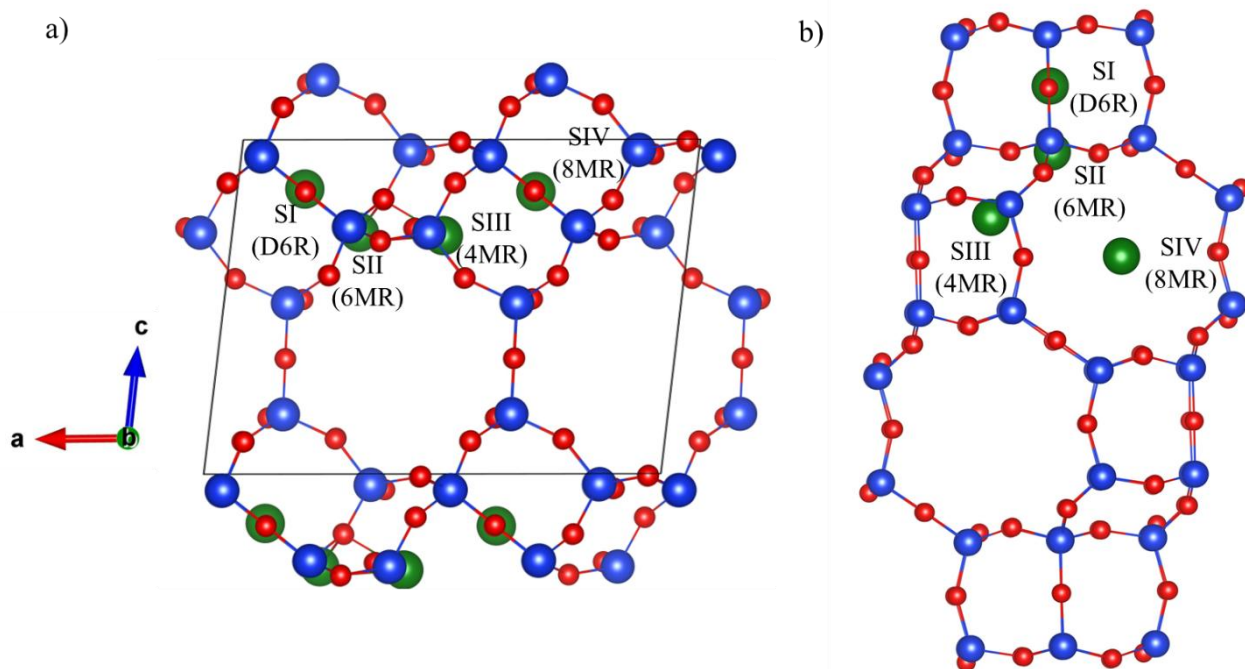


Figure 1. Supercell of chabazite used in the simulations a) Front view. b) Side view showing the supercage of chabazite. Color code: Si in blue, O in red, extra-framework cationic sites SI to SIV are depicted in green.

Computational settings

The calculations have been performed within periodic density functional theory (DFT) using the Vienna *Ab Initio* Simulation Package (VASP) code,^{45–47} with the semilocal Perdew-Burk-Ernzerhof (PBE) functional⁴⁸. The Kohn-Sham equations⁴⁹ were solved using the projector augmented plane wave (PAW) method developed by Blöchl⁵⁰ and adjusted by Kresse and Joubert.⁵¹ As we have used a large supercell, sampling of the Brillouin zone was limited to the Γ -point. The convergence criterion for the electronic self-consistent cycle was set 10^{-6} eV and the plane wave cutoff kinetic energy to 500 eV. The atomic positions were fully relaxed until all forces were smaller than 0.02 eV/Å per atom.

The long-range dispersion interactions are crucial for an accurate description of gas molecule adsorption in zeolites. They have been computed using the Tkatchenko-Scheffler scheme with iterative Hirshfeld partitioning (TS/Hi).^{52–54} This method has demonstrated good accuracy in various zeolites applications.^{34,55} The Hubbard-like U parameter⁵⁶ was applied to improve the

description of localized d states of the Fe^{2+} cation, with Hubbard parameters U_{eff} and J of 4.0 eV and 1.0 eV respectively, derived from Wang et al.⁵⁷ Spin-polarized (collinear) calculations were performed for systems containing Fe^{2+} and Cu^{2+} . Both cations were found energetically more stable in the high spin state with a spin multiplicity of 5 and 2, respectively, in agreement with previous findings.⁵⁸

The adsorption energies of molecules in chabazite at $T = 0$ K were determined from static DFT calculations using the following equation:

$$\Delta E_{ads} = E_{CHA+mol} - E_{CHA} - E_{mol}, \quad \text{Eq. 1}$$

where E_{CHA} is the energy of chabazite, E_{mol} the energy of the isolated molecule in gas phase and $E_{CHA+mol}$ the energy of the adsorbed molecule in chabazite.

In the same way the contribution of dispersion energies ΔE_{disp} to the total interaction energy was obtained by:

$$\Delta E_{disp} = E_{disp,CHA+mol} - E_{disp,CHA} - E_{disp,mol}. \quad \text{Eq. 2}$$

To describe the adsorption phenomena at finite temperature ($T = 300\text{K}$), *ab initio* molecular dynamics (AIMD) simulations have been further performed in the NVT ensemble with the same settings, except for the dispersion correction. Indeed, the TS/HI correction scheme being computationally too costly was exchanged with the D2 dispersion correction of Grimme⁵⁹ which has a good accuracy in zeolite chemistry.⁶⁰ The simulation temperature of 300 K has been maintained by the Andersen thermostat⁶¹ with a collision frequency per atom of 0.01 per step. The integration step was 0.5 fs and we performed runs of at least 100 ps with an equilibration period of at least 10 ps (the production period remaining of at least 90 ps). The convergence of potential energy was carefully checked (with independence of the mean and variance over long period) and the standard error on the mean was estimated after block averaging.⁶²

The finite temperature internal energy of adsorption has been computed as follows:

$$\Delta U_{ads} = \langle E_{CHA-mol} \rangle - \langle E_{CHA} \rangle - \langle E_{mol} \rangle, \quad \text{Eq. 3}$$

where $\langle E_{CHA-mol} \rangle$, $\langle E_{CHA} \rangle$ and $\langle E_{mol} \rangle$ are, respectively, ensemble averages of the total energies of adsorbed molecule in chabazite, the clean chabazite and the molecule in gas phase.

The enthalpy of adsorption was deduced from the internal energy of adsorption by:

$$\Delta H_{ads} = \Delta U_{ads} - RT. \quad \text{Eq. 4}$$

Results and discussion

Stability and distribution of divalent cation sites in chabazite

The distribution and location of divalent extra-framework cations in zeolites is of paramount importance for the optimal formulation of zeolite-based materials for efficient adsorption and catalytic applications.^{28,30,41,63–65} Usually, the stability of cations in specific sites is determined by the electrostatic and chemical interactions of the cations with the oxygen atoms of the framework. However, the distribution of Al atoms in zeolites is known to be strongly influenced by the synthesis conditions employed^{66,67} and is not thermodynamically driven.⁶⁸

The stability of the divalent cations Ca^{2+} , Mg^{2+} , Fe^{2+} , Cu^{2+} , Zn^{2+} , and Sn^{2+} was investigated in the three different sites that are accessible to guest molecules in the chabazite structure (SII to SIV). Site I, located at the center of the D6R prism, was excluded from this comparative analysis due to its limited accessibility to guest molecules as a result of the framework's steric constraints,⁶⁹ which is analogous to the sodalite cages of faujasite.^{70,71} Different possible distributions of the Al positions were considered (Figure 2), following the Löwenstein rule,⁷² which states that the connection of two AlO_4^- tetrahedra via a shared oxygen atom (Al-O-Al bond) is unstable. Therefore, we investigated different possible distributions of two aluminium atoms in the same rings (4MR, 6MR and 8MR), facing the same cavity. These cationic sites are able to accommodate divalent cations.⁷³

Regarding the 4MR site (SIII), only one configuration was considered in which two Al atoms are located in T1 and T2 positions. For the 6MR site (SII), two configurations denoted as 6MR(1-3) and 6MR(1-4) were explored, with the two Al atoms located in T1 and T3 or in T1 and T4 tetrahedral sites and separated, respectively, by one or two Si atoms. As For the 8MR site (SIII'), three possible configurations were considered for the distribution of the two Al atoms. Specifically, the two Al atoms were placed in T1 and T5, T1 and T6, or T1 and T7 positions, denoted as 8MR(1-3), 8MR(1-4) and 8MR(1-5) configurations, respectively, and were separated by one, two, or three Si atoms (Figure 2).

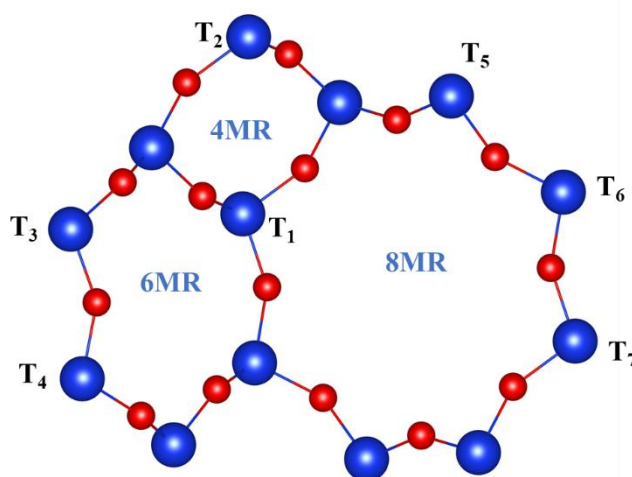


Figure 2. Location of the tetrahedral atoms T1 to T7 in 4MR, 6MR and 8MR rings. Color code: Si in blue, O in red.

Figure 3 displays the relative stabilities of chabazite cells with respect to the cations and Al atoms distributions, with the respective values provided in Table S1. Our results demonstrate that the 6MR site, regardless of the cation type, is the most energetically favorable site, wherein the 1-4 aluminum combination exhibits greater stability as compared to the 1-3 in the 6MR site, followed by the 4MR and 8MR (1-3) sites. The 8MR (1-4) and (1-5) sites show the weakest stability among all sites investigated. The interaction of divalent cations in the 6MR sites (SII) is favored for steric reasons, as the cation is able to interact with three adjacent oxygen atoms of the ring (Figure 4). Notably, these results are in agreement with previous results reported in the literature: the most stable configuration for Cu^{2+} and Co^{2+} in chabazite

is the 6MR (1-4) configuration, with the 6MR (1-3) exhibiting 19 kJ/mol less stability for Cu^{2+} .^{64,73}

Generally speaking, the extra-framework divalent cation distribution in chabazite is still debated. Kwak et al suggested that at low ion exchange levels, Cu^{2+} is coordinated in the 6MR sites, yielding stable species, while it can be found in larger cavities once the most stable sites are saturated.⁷⁴ On the other hand, another computational and experimental study posited that 80% of the Cu(II) cations in CHA are in 8MR sites.⁷⁵ Meanwhile, Göttl et al.⁶⁴ demonstrated by theoretical calculations, in good relation with experimental work, that Cu^{2+} cations preferentially occupy the 6MR sites at the lowest exchange levels, while the 8MR sites remain unoccupied even at high exchange levels. These 6MR sites are believed to be responsible for the catalytic reduction of nitrous oxides.

As for the distribution of Al atoms in chabazite extra framework, it has been demonstrated that the 8MR (1-5) configuration, corresponding to the Al-O-(Si-O)₃-Al sequence (Figure 4), can only accommodate divalent cations at the highest loadings.⁷³ This configuration is by far the least stable in our calculations (except for Sn^{2+}). Therefore, it was excluded from the calculations of adsorption energies.

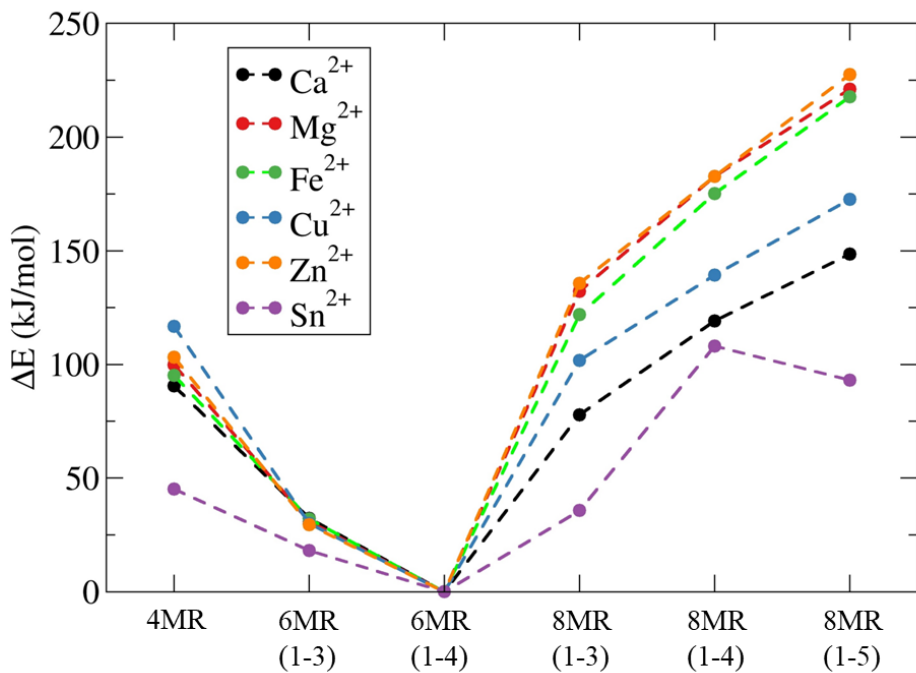


Figure 3. Computed relative stability ΔE (in kJ/mol) of cation exchanged chabazites, with divalent cations in different sites (4MR, 6MR and 8MR), and with different distributions of aluminium atoms. For each series, the structure of lowest energy (6MR (1-4)) is chosen as reference.

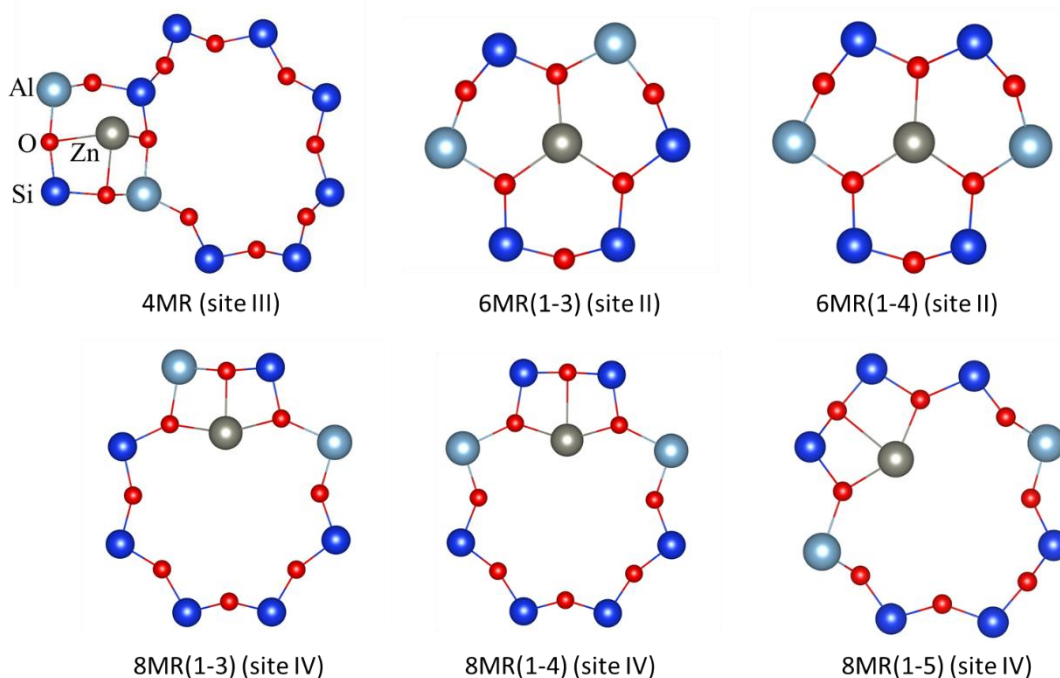


Figure 4. Equilibrium configurations for a divalent cation (Zn^{2+}) in the different sites investigated.

Adsorption of CO₂, CH₄, N₂ and H₂ in exchanged chabazite

To evaluate the potential of cation exchanged chabazites to purify biogas by selective adsorption, the electronic energies of adsorption ΔE_{ads} (Eq. 1) of CH₄, CO₂, N₂ and H₂ were conducted on different sites of divalent cation exchanged chabazites. The results are shown in Figure 5 and the computed values are reported together with the contribution of dispersion energies in Table S2 of the Supporting Information. Additionally, the optimized structures after adsorption of the four gases in 6MR (1-4) and 8MR (1-3) sites are depicted in Figures S1 and SII of the Supporting Information.

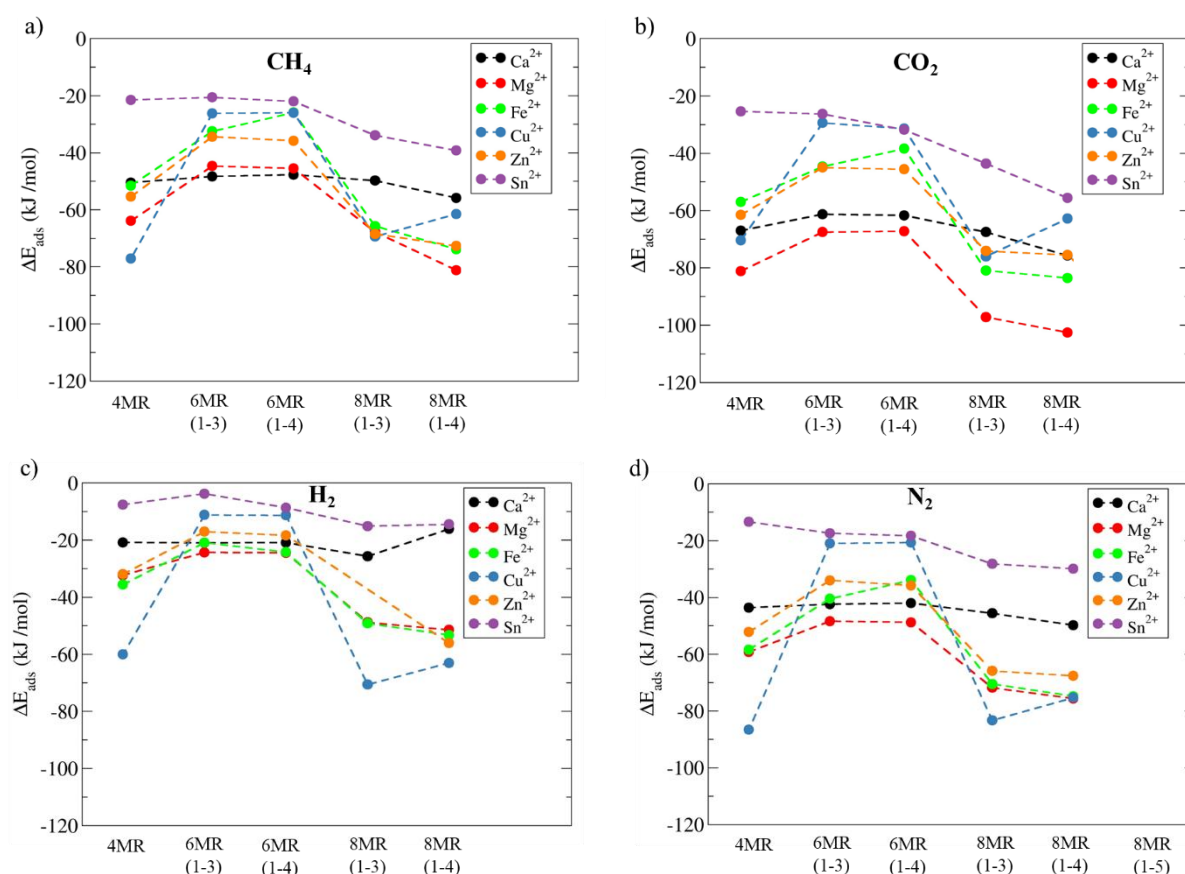


Figure 5. Computed adsorption energies of a) CH₄, b) CO₂, c) H₂ and d) N₂ on the various sites of CHA exchanged with Ca²⁺, Mg²⁺, Fe²⁺, Cu²⁺, Zn²⁺ and Sn²⁺.

For all cation exchanged chabazites, the adsorption of all four molecules investigated is exothermic over all the sites ($\Delta E_{ads} < 0$). As anticipated in the literature,^{41,76} the adsorption energies of the chabazites exchanged by Mg²⁺, Fe²⁺, Cu²⁺ and Zn²⁺ follow the inverse order of

the cation stability: the less stable the cation position, the higher (in absolute value) the interaction energy. The 4MR and 8MR sites display the highest adsorption energies (ΔE_{ads} , in absolute values), followed by the 6MR site which exhibits the lowest affinity for the guest molecules. The strongest interaction in the largest 8MR sites arises from the fact that the guest molecules can approach the cations more closely (see Table S4 in Supporting Information). This trend is less pronounced for the largest cations, Ca^{2+} and Sn^{2+} (100 and 122 pm of ionic radii, respectively, see Table S5), although the interaction of the guest molecule with the 8MR (1-3) or (1-4) site is still the strongest. For all guest molecules, Sn^{2+} displays the lowest adsorption energies, with the values in Table S2 indicating that the interaction of gas molecules on Sn^{2+} is primarily controlled by long range dispersion interactions.

For CH_4 adsorption, Mg-CHA is the best adsorbent with an average adsorption energy of -60.6 kJ/mol on all sites, whereas Sn-CHA is found to be the least effective adsorbent, exhibiting an average adsorption energy of -27.4 kJ/mol. The other cations displayed a comparable behavior, with average adsorption energies of approximately -50 kJ/mol (-50.4 for Ca^{2+} , -49.9 for Fe^{2+} , -52.0 for Cu^{2+} and -53.4 for Zn^{2+}). As expected from a non-polar molecule, the dispersion energy contribution is significant, ranging from 36% to 50% of the total adsorption energy, see Table S2. Notably, these values are consistent (within 10 kJ/mol) with the findings of Barbosa et al⁴¹ who reported an adsorption energies in Zn-CHA of -11.1 kJ/mol in 6MR, -37.7 kJ/mol in 8MR, and -44.8 kJ/mol in 4MR. It should be noted that the reported values were obtained using the PW91 function without accounting for the energy dispersion correction. For a comparison, our PBE values are provided in Table S2.

In the case of CO_2 adsorption, the molecule interacts with all cations through its oxygen atom as depicted in Figures S1 and S2. Similar to the behavior observed for the CH_4 adsorption,

with, in general, a stronger interaction. Mg-CHA represents the most adsorption-sensitive cation with a calculated average interaction energy across all sites of -83.1 kJ/mol, accompanied by dispersion energy contribution of -18.1 kJ/mol. On average, these interaction energies decrease for Ca-CHA by about ~20 kJ/mol. Such a decrease is consistent with a simple electrostatic picture,³³ the larger Ca²⁺ cation being less polarizing than Mg²⁺ (see the ionic radii in Table S5). As a consequence, the average distance between the oxygen atom of CO₂ and the alkaline earths cations increases from Mg²⁺ (d = 2.078 Å) to Ca²⁺ (d = 2.422 Å, see Table S4). The weakest interaction is observed for Sn-CHA with an average adsorption energy of -36.5 kJ/mol, characterized by the longest CO₂-cation distance (d(CO₂-Sn²⁺) = 3.019 Å on average). For the remaining cations, adsorption energies are around -60 kJ/mol (-60.9 kJ/mol for Fe²⁺, -54 kJ/mol for Cu²⁺ and -60.3 kJ/mol for Zn²⁺ in average). These results are in agreement with Sangthong's findings on CO₂ adsorption on 6MR sites of faujasite, where adsorption energies of -66.5 and -46.9 kJ/mol were obtained for Zn(II) and Cu(II) respectively.⁷⁷ Furthermore, Li et al. computed adsorption energies in the 6MR of divalent cation-exchanged Y zeolite to be -61.5 kJ/mol for MgY, and -48.9 kJ/mol for CaY.⁷⁸ These CO₂ adsorption energies are also stronger than those computed on monovalent metal cation-exchanged chabazite (-26 to -52 kJ/mol for K to Li-CHA).⁷⁸

For N₂, once again the adsorption is more favorable on Mg-CHA with an average interaction energy across all adsorption sites of -60.8 kJ/mol. Sn-CHA, on the other hand, displays the weakest interaction, with an average adsorption energy of -21.5 kJ/mol. The remaining cation-exchanged chabazites exhibit intermediate adsorption energies, with Fe²⁺, Cu²⁺, Zn²⁺, and Ca²⁺ having average interaction energies of -55.6 kJ/mol, -57.4 kJ/mol, -51.1 kJ/mol, and -44.7 kJ/mol, respectively. It is worth noting that our computed interaction energies for Ca-CHA are 16 kJ/mol higher than those reported in a previous study by Mikosch,⁷⁹ who incorporated Ca cations in small clusters rather than a periodic cell, as in our case. This

difference in energy may be attributed to the effect of confinement in bulk phase compared to clusters, as reported in previous studies.⁸⁰

Dihydrogen (H_2) presents a special case since this molecule's adsorption can lead to dissociation upon some cations, resulting in the formation of an acid bridging site on the zeolite structure (Si-OH-Al) and a metal hydride. In a separation process, this dissociative adsorption can complicate the material regeneration process. Our findings indicate that non-dissociative adsorption of H_2 is possible on all sites and for all cations except for the 8MR(1-3) site of Zn-CHA, where a spontaneous dissociation occurs. When forcing a dissociative adsorption, we observed an exothermic adsorption on Mg, Fe, Cu, and Zn-CHA (see Table S3 in the Supporting Information). Therefore, these cation-exchanged chabazites may not be suitable for the selective dihydrogen adsorption. Both H_2 adsorption modes upon Mg-CHA are depicted in Figure S2. Sn^{2+} displays an intermediate case, where dissociative H_2 adsorption is endothermic while the molecular adsorption is slightly exothermic (averaging at -9.9 kJ/mol). For Ca^{2+} , the average molecular H_2 adsorption energy is -20.9 kJ/mol and we were unable to optimize dissociated dihydrogen on Ca-CHA. Dissociative adsorption of dihydrogen has been reported in 8MR sites of Zn^{2+} -mordenite⁶³ and MOR, as well as for Zn^{2+} -chabazite⁸¹ and was shown to be more favorable than the molecular adsorption depending on the relative positions of the Al atoms in the 8MR. For the H_2 molecular adsorption, similar values to our findings were computed in the LTA-type zeolite substituted with Ca^{2+} (Ca-A), at the PBE level they reported an adsorption energies of -10.5 kJ/mol in 6MR and -22.9 kJ/mol in 8MR.⁸² These results suggest that careful consideration should be taken when selecting a zeolite material for the adsorption of dihydrogen, as the dissociative or non-dissociative adsorption mode may impact the material regeneration process.

Separation of binary mixtures of CO₂, CH₄, N₂ and H₂

In this section, we aim to identify the most appropriate cation for the selective adsorption of interest in terms of thermodynamic selectivity, by analyzing the difference in adsorption energies ($\Delta\Delta E_{ads}$) on various cation-exchanged chabazites. This analysis will be useful for identifying the most suitable adsorbent for specific separation processes, the results are illustrated in Figure 6 for CH₄ purification, Figure 7 for H₂ purification, and Figure 8 for CO₂/N₂ separation. Thermodynamic adsorption selectivity is excellent with difference of adsorption energies greater than 15 kJ/mol (the corresponding Boltzmann factor $\exp\left(-\frac{15 \times 10^3}{RT}\right) \approx 2.5 \times 10^{-3}$ becoming much smaller than 1).

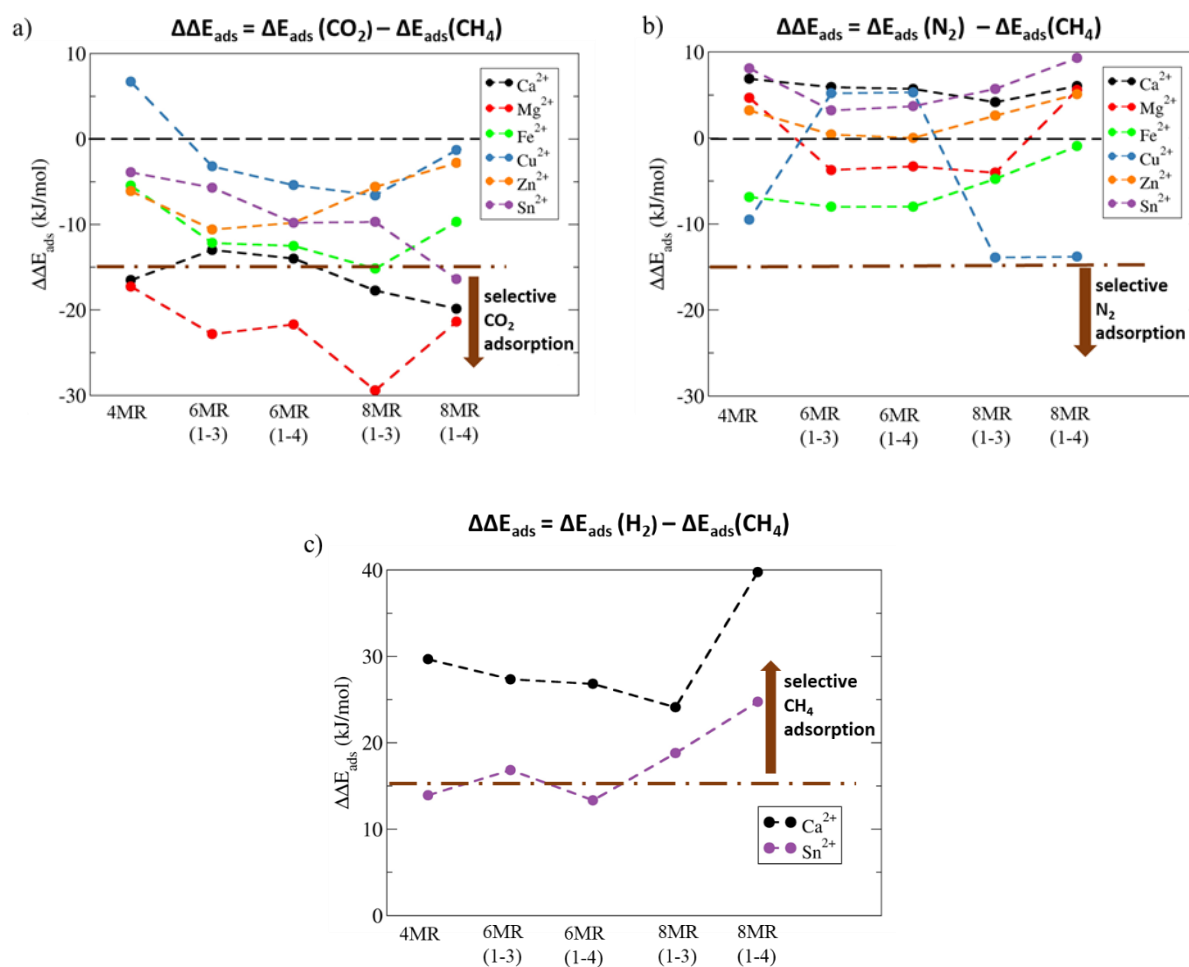


Figure 6. Difference of adsorption energies of the gases investigated for CH₄ purification on the series of divalent cation exchanged chabazites. Difference between CO₂ and CH₄ (a), N₂ and CH₄ (b) and H₂ and CH₄ (c).

Purification of CH₄ rich mixtures

In this section, we explore the feasibility of purifying a CH₄ rich mixture in the presence of impurities such as CO₂, N₂ and H₂. We analyze the differences $\Delta\Delta E_{\text{ads}}$ in adsorption energies between CH₄ and the impurities CO₂, N₂, and H₂ as presented in Figure 6(a-c). Negative values indicate a higher affinity of the cation-exchanged chabazite for the impurity (CO₂, N₂ or H₂) than for CH₄.

Figure 6.a highlights that alkaline earth cations, Ca²⁺ and above all Mg²⁺, are the most promising cations for the removal of CO₂ from CH₄. On transition metal cations, CO₂ interaction is always stronger, albeit the CO₂/CH₄ separation is less convincing. This stronger adsorption of CO₂ than CH₄ is related to the permanent electric quadrupole moment of CO₂, which is responsible for stronger electrostatic interactions with the extra-framework cations, whereas CH₄ is apolar.⁸³

For N₂/CH₄ separation, it is well known that the superior polarizability of CH₄ favors a strong interaction with the adsorbent when compared to N₂.³ Indeed, the difference in adsorption energies shows a slight preferential adsorption (~0 to +10 kJ/mol) for CH₄ when interacting on Ca^{II}, Zn^{II}, Sn^{II} and certain sites of Mg^{II} and Cu^{II}-CHA. In contrast, for Fe^{II} and specifically for Mg^{II} and Cu^{II}-CHA sites, a preferential adsorption of N₂ is observed. Nevertheless, all of these energy differences are moderate, pointing to the poor performance of the studied divalent cations for N₂/CH₄ separation.

For H₂/CH₄ separation, Ca²⁺ and Sn²⁺ are the most promising cations for this separation, as they do not dissociate H₂ upon adsorption (see Section 3.2). However, the $\Delta\Delta E_{\text{ads}}$ analysis depicted in see Figure 6.c, show that the CH₄ interaction is always stronger than that of H₂,

making the investigated divalent cations not suitable for purification of CH₄ rich mixtures of its potential H₂ impurity.

As a conclusion of this section, the most promising separation that could be achieved is CO₂/CH₄ on Mg-CHA. To complement these reported static investigations at T = 0 K, molecular dynamics simulations were performed at finite temperature (T = 300 K) and the results are reported in Section 3.4.

Purification of H₂ rich mixtures

In the context of steam methane reforming, CO₂, CH₄, and N₂ are among the main impurities in dihydrogen.³ In order to identify the cations that could enable the obtain of an highly pure H₂ product, we report the differences in adsorption energies of CO₂-H₂, and N₂-H₂ on Ca²⁺ and Sn²⁺ exchanged chabazites, see Figure 7. It is worth noting that Ca²⁺ and Sn²⁺ are the only cations in our series that do not dissociate H₂ upon adsorption.

The displayed results show that CO₂ interacts more strongly than H₂ on both cations-exchanged chabazites. Specifically, Ca²⁺ yields the largest differences in adsorption energies between CO₂ and H₂ (Figure 7.a). N₂ is also preferentially adsorbed over H₂ on Ca²⁺-CHA, while Sn²⁺ being less efficient in this regard (Figure 7.b). Based on these findings, we propose Ca²⁺-CHA as a promising adsorbent for H₂ purification.

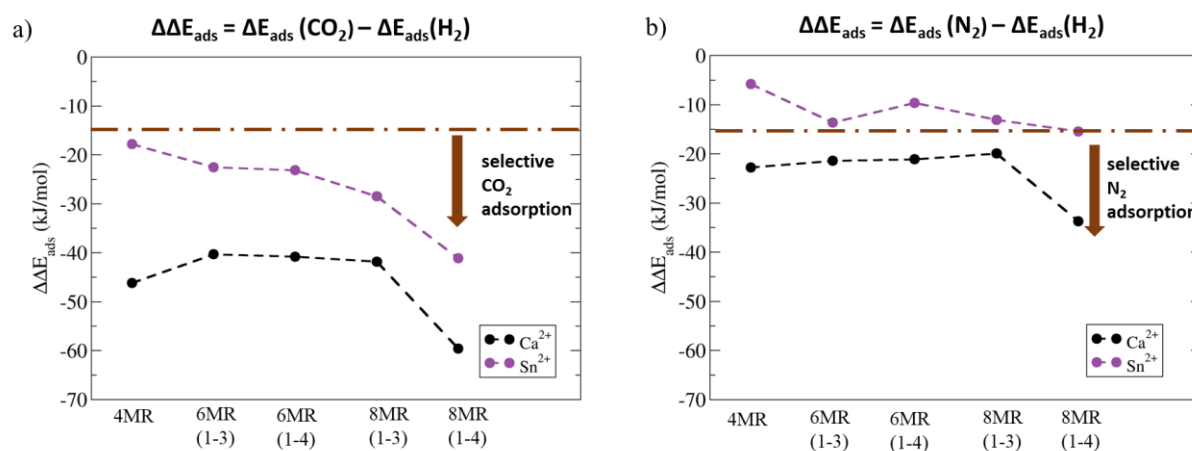


Figure 7. Difference of adsorption energies of the gases investigated for H₂ purification on Ca and Mg exchanged chabazites. Difference between CO₂ and H₂ (a), N₂ and H₂ (b).

CO₂/N₂ separation

The removal of CO₂ from post-combustion gases that are rich in N₂ is an essential step for their treatment. The traditional techniques for this process is amine scrubbing, and most of the research on zeolite adsorbents has focused on the FAU and LTA zeolites exchanged with monovalent cations.³ Among them, NaX (FAU structure) is considered as the benchmark adsorbent. For alkaline earth cations Ca²⁺ and Mg²⁺, it can be seen from Figure 6.c that the interaction of CO₂ is more favorable than that of N₂, with a difference of adsorption energies much larger than 15 kJ/mol in absolute value. Therefore, this observation suggests that chabazites exchanged with Ca and Mg could be potentially useful for the selective removal of CO₂ from N₂.

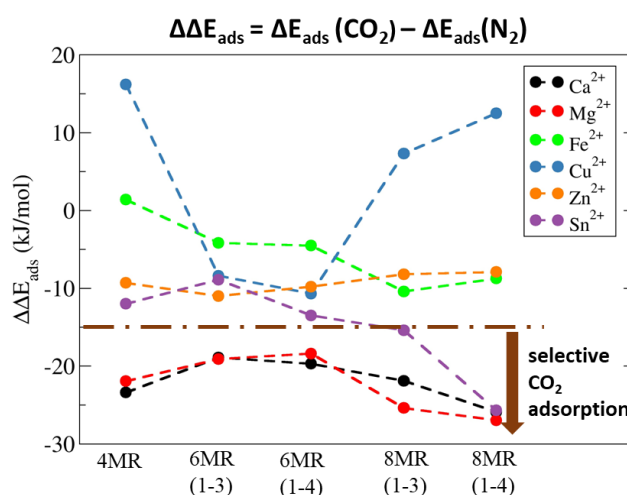


Figure 8. Difference of adsorption energies of CO₂ and N₂ on divalent cation exchanged chabazites.

Co-adsorption CO₂/CH₄ at finite T

In the context of biogas purification, the separation of CO₂ from CH₄-rich mixtures has been identified as the most promising application of Mg-CHA, based on static calculations performed at T = 0 K. In order to investigate the behavior of the adsorbent at a finite temperature, *ab initio* Molecular Dynamics (AIMD) simulations were carried out to calculate the adsorption energies ΔU_{ads} and enthalpies ΔH_{ads} at T = 300 K. The finite temperature

internal energy of adsorption ΔU_{ads} is computed from ensemble averages of the total energies (Eq. 3) and can be used for comparison with electronic energies of adsorption ΔE_{ads} computed by static DFT calculations. ΔH_{ads} is useful to let further comparison with experimental data determined at given temperature and pressure.

For reasons of computational cost, AIMD simulations were performed at the PBE+D2 level of theory (see Section 2.2). The consistency between the PBE+D2 dispersion correction and the more elaborate PBE+TS/HI used in the previous sections was checked by calculations of ΔE_{ads} by static periodic DFT calculations. The results of these two calculations differs by only 1 to 7 kJ/mol (see Table 1), which confirms that the PBE+D2 level of theory can be safely used in the AIMD simulations.

Adsorption energies (ΔU_{ads}) obtained via AIMD simulations at 300K follow the same trend as electronic adsorption energies (at $T = 0\text{K}$) computed by static periodic DFT calculations (see Table 1). On the 6MR site, adsorption energies (ΔU_{ads}) obtained at 300 K for Mg-CHA differs from electronic adsorption energies (at $T = 0\text{K}$) at the same PBE+D2 level of theory only by 3 kJ/mol for CO_2 adsorption and by 8 kJ/mol for CH_4 adsorption, which shows that thermal effects are not very important for this site which is sterically constrained. However, at the 8MR site, the static results are overestimated by about 17 kJ/mol for CO_2 and 11 kJ/mol for CH_4 , in absolute value (see Table 1). As expected on this more accessible site, thermal effects are more important. Despite this, the differences in adsorption enthalpies ($\Delta H_{ads}(\text{CO}_2) - \Delta H_{ads}(\text{CH}_4)$) at both sites (-20 ± 6 kJ/mol for 6MR and -25 ± 4 kJ/mol for 8MR) are remarkably close to the differences in static energies of adsorption calculated at $T = 0$ K (-18.7 kJ/mol for 6MR and -29.4 kJ/mol for 8MR) using PBE+TS/HI level of theory which allows us to conclude that the conclusions drawn in Sections 3.2 and 3.3 from calculations at $T = 0$ K can be generalized at finite temperature.

To investigate the possible inhibitory effect of CH₄ concentration on CO₂ adsorption, we conducted AIMD simulations featuring co-adsorption of CO₂ (1 molecule) and CH₄ (1 to 4 molecules) at the 6MR(1-4) and 8MR(1-3) sites of Mg-CHA. Two different initial configurations were tested in the runs with one CO₂ and one CH₄, with CO₂ adsorbed on Mg and CH₄ far from Mg, and vice versa. The two situations led to similar final states. For steric reasons, the 6MR(1-4) site can accommodate only one molecule and CO₂ is adsorbed on Mg while CH₄ is far from Mg. On the 8MR(1-3) site, both sides of the 8MR are accessible and both molecules are adsorbed, one on each side. As in the final states, CO₂ is adsorbed on Mg, three more CH₄ molecules were added in these configurations to prepare the initial states with 1 CO₂ and 4 CH₄. More details are given in Supporting Information (Section S2, Figures S3 to S5 for the simulations on the 6MR(1-4) site and Figures S6 to S8 for the simulations on the 8MR(1-3) site).

Figure 9.a. displays the radial distribution functions of the distance between the cation (Mg) and the interacting O (CO₂) atom. The observed peaks at 2.12, 2.11, and 2.10 Å for the 6MR site, and 2.02, 2.04 and 2.06 Å for the 8MR site of the Mg-O(CO₂) in the presence of 0, 1, and 4 molecules of CH₄, respectively, indicate that the interaction between CO₂ with Mg remains unaffected, and that the presence of CH₄ has a negligible impact on the adsorption of CO₂ on Mg-CHA.

The findings presented in this section provide further support for the previous prediction obtained using static calculations, namely that Mg-CHA is an excellent candidate for capturing CO₂ in CH₄ rich mixtures at 300 K.

		ΔE_{ads} (kJ/mol) Static PBE+TS/Hi	ΔE_{ads} (kJ/mol) Static PBE+D2	ΔU_{ads} (kJ/mol) MD, 300K, PBE+D2	ΔH_{ads} (kJ/mol) MD, 300K PBE+D2
Mg-CHA 6MR(1-4)	CH ₄	-50.3	-54.1	-46.4 ± 3.5	-48.9 ± 3.5
	CO ₂	-68.7	-69.3	-66.4 ± 3.5	-68.9 ± 3.5
Mg-CHA 8MR(1-3)	CH ₄	-67.8	-69.7	-53.1 ± 3.1	-55.6 ± 3.1
	CO ₂	-97.2	-104.5	-77.7 ± 3.1	-80.2 ± 3.1

Table 1. Calculated adsorption energies for CH₄ and CO₂ in the 6MR(1-4) and 8MR(1-3) sites of Mg-CHA, by static calculations (T = 0 K) and *ab initio* Molecular Dynamics simulations (T = 300 K).

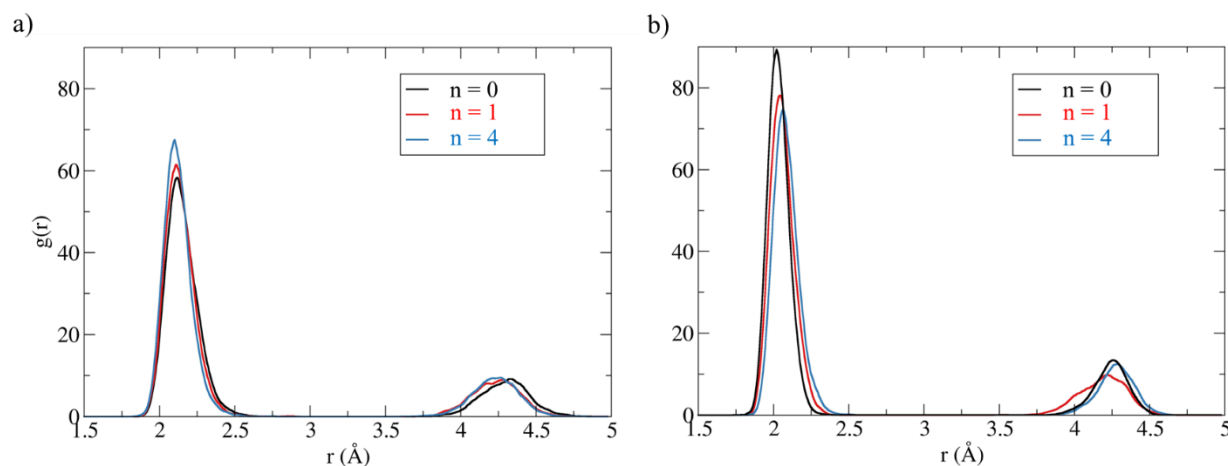


Figure 9. Radial pair distribution functions between the Mg²⁺ cation and the O atoms of CO₂ in presence of *n* molecules of CH₄ inside the large cavity of Mg-CHA (*n* = 0 in black, *n* = 1 in red and *n* = 4 in blue) for Mg²⁺ in the 6MR(1-4) site (a) and 8MR(1-3) site (b).

Conclusions

The adsorption and separation capacities of various divalent cations-exchanged chabazites were investigated by periodic DFT calculations, with TS/HI correction of dispersion. The stability of these divalent cations (Mg²⁺, Ca²⁺, Fe²⁺, Cu²⁺, Zn²⁺ and Sn²⁺) was demonstrated in 6MR with pairs of aluminium atoms in T1 and T4 tetrahedral sites, separated by two Si atoms (Section 3.1). All the cationic adsorption sites were subsequently explored to describe the diversity of sites in the typical experimental chabazite of Si/Al ratio close to 2 or 3. The results revealed that the chosen cations are not suitable for preferential capture of N₂ and H₂ in the purification of CH₄ rich mixtures. However, Mg-CHA was identified as the most promising cation for the selective adsorption of CO₂. These predictions were further supported by *ab initio* molecular dynamics simulations at 300 K (Section 3.4). The co-adsorption of CH₄ and CO₂ on Mg-CHA was also investigated, and the results showed that the presence of CH₄ has a negligible impact on the adsorption of CO₂ on Mg-CHA.

Regarding the selective adsorption of CO₂ in N₂ rich post combustion gases, our results indicate that Ca and Mg exchanged chabazites could be useful for the selective CO₂ removal. Finally, for the purification of H₂ rich mixtures, Ca²⁺ and Sn²⁺ are the only cations that did not dissociate H₂ and may therefore have potential use cases. In particular, Ca²⁺ is the most favorable cation for selective adsorption of H₂ and CO₂.

Overall, these findings provide valuable insights into the factors influencing the adsorption behavior of N₂, H₂, CH₄, and CO₂ on divalent cation-exchanged zeolites, which can be useful for the design and development of efficient adsorbents for gas separation and purification applications. Importantly, this study highlights the crucial role that theoretical calculations and simulations can play in facilitating and supporting experimental work by providing clear guidelines on framework and cation compositions, and allowing for deeper understanding of fundamental questions regarding the cations distribution and preferential sites of adsorption within the CHA zeolite.

Supporting Information

S1. Static calculations

Tables of numerical results of sections 3.1 to 3.3.

Figures of a selection of structures of different molecules adsorbed in Mg-exchanged chabazite, in 6MR(1-4) and 8MR(1-3) sites.

S2. Co-adsorption CO₂/CH₄ at finite T

Figures illustrating the MD simulations of co-adsorption with one CO₂ and one CH₄ adsorbed in Mg-CHA.

Acknowledgments

This work was funded by the Normandy region through the “RIN recherche Chair of Excellence” H4Clean H2oriZEOn. This work was granted access to the HPC resources of TGCC under the allocation 2022-A0120810433 and 2023-A0140810433 made by GENCI. VV and RGN acknowledge the sponsorship of TotalEnergies and Region of Normandy for the project EcoGas.

References

- (1) Fu, D.; Park, Y.; Davis, M. E. Zinc Containing Small- Pore Zeolites for Capture of Low Concentration Carbon Dioxide. *Angew Chem Int Ed* **2022**, *61* (5). <https://doi.org/10.1002/anie.202112916>.
- (2) Ghojavand, S.; Coasne, B.; Clatworthy, E. B.; Guillet-Nicolas, R.; Bazin, P.; Desmurs, M.; Jacobo Aguilera, L.; Ruaux, V.; Mintova, S. Alkali Metal Cations Influence the CO₂ Adsorption Capacity of Nanosized Chabazite: Modeling vs Experiment. *ACS Appl. Nano Mater.* **2022**, *5* (4), 5578–5588. <https://doi.org/10.1021/acsnm.2c00537>.
- (3) Pérez-Botella, E.; Valencia, S.; Rey, F. Zeolites in Adsorption Processes: State of the Art and Future Prospects. *Chem. Rev.* **2022**. <https://doi.org/10.1021/acs.chemrev.2c00140>.
- (4) Yang, J.; Liu, J.; Liu, P.; Li, L.; Tang, X.; Shang, H.; Li, J.; Chen, B. K- Chabazite Zeolite Nanocrystal Aggregates for Highly Efficient Methane Separation. *Angewandte Chemie Intl Edit* **2022**, *61* (8). <https://doi.org/10.1002/anie.202116850>.
- (5) Liu, S.; Shui, J. Mechanism and Properties of Emerging Nanostructured Hydrogen Storage Materials. *Battery Energy* **2022**, 20220033. <https://doi.org/10.1002/bte2.20220033>.
- (6) Sholl, D. S.; Lively, R. P. Seven Chemical Separations to Change the World. *Nature* **2016**, *532* (7600), 435–437. <https://doi.org/10.1038/532435a>.
- (7) *Zeolites in Industrial Separation and Catalysis*, 1st ed.; Kulprathipanja, S., Ed.; Wiley, 2010. <https://doi.org/10.1002/9783527629565>.
- (8) Vermeiren, W.; Gilson, J.-P. Impact of Zeolites on the Petroleum and Petrochemical Industry. *Top. Catal.* **2009**, *52* (9), 1131–1161. <https://doi.org/10.1007/s11244-009-9271-8>.
- (9) Ennaert, T.; Van Aelst, J.; Dijkmans, J.; De Clercq, R.; Schutyser, W.; Dusselier, M.; Verboekend, D.; Sels, B. F. Potential and Challenges of Zeolite Chemistry in the Catalytic Conversion of Biomass. *Chem. Soc. Rev.* **2016**, *45* (3), 584–611. <https://doi.org/10.1039/C5CS00859J>.
- (10) Iyoki, K.; Kikumasa, K.; Onishi, T.; Yonezawa, Y.; Chokkalingam, A.; Yanaba, Y.; Matsumoto, T.; Osuga, R.; Elangovan, S. P.; Kondo, J. N.; Endo, A.; Okubo, T.; Wakihara, T. Extremely Stable Zeolites Developed via Designed Liquid-Mediated Treatment. *J. Am. Chem. Soc.* **2020**, *142* (8), 3931–3938. <https://doi.org/10.1021/jacs.9b12709>.
- (11) Takata, T.; Tsunoji, N.; Takamitsu, Y.; Sadakane, M.; Sano, T. Nanosized CHA Zeolites with High Thermal and Hydrothermal Stability Derived from the Hydrothermal Conversion of FAU Zeolite. *Microporous and Mesoporous Materials* **2016**, *225*, 524–533. <https://doi.org/10.1016/j.micromeso.2016.01.045>.
- (12) Baerlocher, C.; McCusker, L. B. *Database of Zeolite Structures*. <http://www.iza-structure.org/databases/> (accessed 2022-09-26).
- (13) Dusselier, M.; Davis, M. E. Small-Pore Zeolites: Synthesis and Catalysis. *Chem. Rev.* **2018**, *118* (11), 5265–5329. <https://doi.org/10.1021/acs.chemrev.7b00738>.
- (14) Sircar, S. Drying Processes. In *Handbook of Porous Solids*; Schth, F., Sing, K. S. W., Weitkamp, J., Eds.; Wiley-VCH Verlag GmbH: Weinheim, Germany, 2002; pp 2533–2567. <https://doi.org/10.1002/9783527618286.ch32>.
- (15) van Speybroeck, V.; Hemelsoet, K.; Joos, L.; Waroquier, M.; Bell, R. G.; Catlow, C. R. A. Advances in Theory and Their Application within the Field of Zeolite Chemistry. *Chem. Soc. Rev.* **2015**, *44* (20), 7044–7111. <https://doi.org/10.1039/c5cs00029g>.
- (16) Cnudde, P.; Demuynck, R.; Vandenbrande, S.; Waroquier, M.; Sastre, G.; Speybroeck, V. V. Light Olefin Diffusion during the MTO Process on H-SAPO-34: A Complex

- Interplay of Molecular Factors. *J. Am. Chem. Soc.* **2020**, *142* (13), 6007–6017. <https://doi.org/10.1021/jacs.9b10249>.
- (17) Breck, D. W. *Zeolite Molecular Sieves: Structure, Chemistry, and Use*; John Wiley and Sons: New York, 1975; Vol. 13.
- (18) Zhang, J.; Singh, R.; Webley, P. A. Alkali and Alkaline-Earth Cation Exchanged Chabazite Zeolites for Adsorption Based CO₂ Capture. *Microporous and Mesoporous Materials* **2008**, *111* (1–3), 478–487. <https://doi.org/10.1016/j.micromeso.2007.08.022>.
- (19) Rivera-Ramos, M. E.; Ruiz-Mercado, G. J.; Hernández-Maldonado, A. J. Separation of CO₂ from Light Gas Mixtures Using Ion-Exchanged Silicoaluminophosphate Nanoporous Sorbents. *Ind. Eng. Chem. Res.* **2008**, *47* (15), 5602–5610. <https://doi.org/10.1021/ie071309v>.
- (20) Rivera-Ramos, M. E.; Hernández-Maldonado, A. J. Adsorption of N₂ and CH₄ by Ion-Exchanged Silicoaluminophosphate Nanoporous Sorbents: Interaction with Monovalent, Divalent, and Trivalent Cations. *Ind. Eng. Chem. Res.* **2007**, *46* (14), 4991–5002. <https://doi.org/10.1021/ie061016m>.
- (21) Shang, J.; Li, G.; Singh, R.; Xiao, P.; Liu, J. Z.; Webley, P. A. Determination of Composition Range for “Molecular Trapdoor” Effect in Chabazite Zeolite. *J. Phys. Chem. C* **2013**, *117* (24), 12841–12847. <https://doi.org/10.1021/jp4015146>.
- (22) Shang, J.; Li, G.; Gu, Q.; Singh, R.; Xiao, P.; Liu, J. Z.; Webley, P. A. Temperature Controlled Invertible Selectivity for Adsorption of N₂ and CH₄ by Molecular Trapdoor Chabazites. *Chem. Commun.* **2014**, *50* (35), 4544. <https://doi.org/10.1039/c4cc00269e>.
- (23) Shang, J.; Li, G.; Singh, R.; Gu, Q.; Nairn, K. M.; Bastow, T. J.; Medhekar, N.; Doherty, C. M.; Hill, A. J.; Liu, J. Z.; Webley, P. A. Discriminative Separation of Gases by a “Molecular Trapdoor” Mechanism in Chabazite Zeolites. *J. Am. Chem. Soc.* **2012**, *134* (46), 19246–19253. <https://doi.org/10.1021/ja309274y>.
- (24) Debost, M.; Klar, P. B.; Barrier, N.; Clatworthy, E. B.; Grand, J.; Laine, F.; Brázda, P.; Palatinus, L.; Nesterenko, N.; Boullay, P.; Mintova, S. Synthesis of Discrete CHA Zeolite Nanocrystals without Organic Templates for Selective CO₂ Capture. *Angew. Chem. Int. Ed.* **2020**, *59* (52), 23491–23495. <https://doi.org/10.1002/anie.202009397>.
- (25) Ferrari, A. M.; Neyman, K. M.; Huber, S.; Knözinger, H.; Rösch, N. Density Functional Study of Methane Interaction with Alkali and Alkaline-Earth Metal Cations in Zeolites. *Langmuir* **1998**, *14* (19), 5559–5567. <https://doi.org/10.1021/la980017j>.
- (26) Moretti, G.; Ferraris, G.; Fierro, G.; Jacono, M.; Morpurgo, S.; Faticanti, M. Dimeric Cu(I) Species in Cu-ZSM-5 Catalysts: The Active Sites for the NO Decomposition. *Journal of Catalysis* **2005**, *232* (2), 476–487. <https://doi.org/10.1016/j.jcat.2005.03.020>.
- (27) Morpurgo, S.; Moretti, G.; Bossa, M. A Computational Study on N₂ Adsorption in Cu-ZSM-5. *Phys. Chem. Chem. Phys.* **2007**, *9* (3), 417–424. <https://doi.org/10.1039/B608411G>.
- (28) Chebbi, M.; Chibani, S.; Paul, J.-F.; Cantrel, L.; Badawi, M. Evaluation of Volatile Iodine Trapping in Presence of Contaminants: A Periodic DFT Study on Cation Exchanged-Faujasite. *Microporous and Mesoporous Materials* **2017**, *239*, 111–122. <https://doi.org/10.1016/j.micromeso.2016.09.047>.
- (29) Delachaux, F.; Hessou, E. P.; Vallières, C.; Monnier, H.; Badawi, M. A Dispersion-Corrected DFT Method for Zeolite-Based CO₂/N₂ Separation: Assessment and Application. *Journal of Environmental Chemical Engineering* **2023**, *11* (1), 109052. <https://doi.org/10.1016/j.jece.2022.109052>.
- (30) Khalil, I.; Jabraoui, H.; Lebègue, S.; Kim, W. J.; Aguilera, L.-J.; Thomas, K.; Mauge, F.; Badawi, M. Biofuel Purification: Coupling Experimental and Theoretical Investigations for Efficient Separation of Phenol from Aromatics by Zeolites. *Chemical Engineering Journal* **2020**, *402*, 126264. <https://doi.org/10.1016/j.cej.2020.126264>.

- (31) Shang, J.; Li, G.; Singh, R.; Xiao, P.; Danaci, D.; Liu, J. Z.; Webley, P. A. Adsorption of CO₂, N₂, and CH₄ in Cs-Exchanged Chabazite: A Combination of van Der Waals Density Functional Theory Calculations and Experiment Study. *J. Chem. Phys.* **2014**, *11*.
- (32) Kumar, P.; Sung, C.-Y.; Muraza, O.; Cococcioni, M.; Al Hashimi, S.; McCormick, A.; Tsapatsis, M. H₂S Adsorption by Ag and Cu Ion Exchanged Faujasites. *Microporous and Mesoporous Materials* **2011**, *146* (1–3), 127–133. <https://doi.org/10.1016/j.micromeso.2011.05.014>.
- (33) Pirngruber, G. D.; Raybaud, P.; Belmabkhout, Y.; Čejka, J.; Zukal, A. The Role of the Extra-Framework Cations in the Adsorption of CO₂ on Faujasite Y. *Phys. Chem. Chem. Phys.* **2010**, *12* (41), 13534. <https://doi.org/10.1039/b927476f>.
- (34) Daouli, A.; Hessou, E. P.; Monnier, H.; Dziurla, M.-A.; Hasnaoui, A.; Maurin, G.; Badawi, M. Adsorption of NO, NO₂ and H₂O in Divalent Cation Faujasite Type Zeolites: A Density Functional Theory Screening Approach. *Phys. Chem. Chem. Phys.* **2022**, *24* (25), 15565–15578. <https://doi.org/10.1039/D2CP00553K>.
- (35) Hessou, E. P.; Kanhounon, W. G.; Rocca, D.; Monnier, H.; Vallières, C.; Lebègue, S.; Badawi, M. Adsorption of NO, NO₂, CO, H₂O and CO₂ over Isolated Monovalent Cations in Faujasite Zeolite: A Periodic DFT Investigation. *Theor Chem Acc* **2018**, *137* (12), 161. <https://doi.org/10.1007/s00214-018-2373-2>.
- (36) Sung, C.-Y.; Al Hashimi, S.; McCormick, A.; Cococcioni, M.; Tsapatsis, M. A DFT Study on Multivalent Cation-Exchanged Y Zeolites as Potential Selective Adsorbent for H₂S. *Microporous and Mesoporous Materials* **2013**, *172*, 7–12. <https://doi.org/10.1016/j.micromeso.2012.12.006>.
- (37) Chibani, S.; Medlej, I.; Lebègue, S.; Ángyán, J. G.; Cantrel, L.; Badawi, M. Performance of Cu^{II} -, Pb^{II} -, and Hg^{II} -Exchanged Mordenite in the Adsorption of I₂, ICH₃, H₂O, CO, ClCH₃, and Cl₂: A Density Functional Study. *ChemPhysChem* **2017**, *18* (12), 1642–1652. <https://doi.org/10.1002/cphc.201700104>.
- (38) Kington, G. L.; Laing, W. The Crystal Structure of Chabazite and Its Sorptive Properties. *Trans. Faraday Soc.* **1955**, *51*, 287. <https://doi.org/10.1039/tf9555100287>.
- (39) Bučko, T.; Benco, L.; Hafner, J.; Ángyán, J. G. Monomolecular Cracking of Propane over Acidic Chabazite. *J. Catal.* **2011**, *279* (1), 220–228. <https://doi.org/10.1016/j.jcat.2011.01.022>.
- (40) Alberti, A.; Galli, E.; Vezzolini, G.; Passaglia, E.; Zanazzi, P. F. Position of Cations and Water Molecules in Hydrated Chabazite. Natural and Na-, Ca-, Sr- and K-Exchanged Chabazites. *Zeolites* **1982**, *2* (4), 303–309. [https://doi.org/10.1016/S0144-2449\(82\)80075-4](https://doi.org/10.1016/S0144-2449(82)80075-4).
- (41) Barbosa, L. A. M. M.; van Santen, R. A.; Hafner, J. Stability of Zn(II) Cations in Chabazite Studied by Periodical Density Functional Theory. *J. Am. Chem. Soc.* **2001**, *123* (19), 4530–4540. <https://doi.org/10.1021/ja002175e>.
- (42) Civalieri, B.; Ferrari, A. M.; Llundell, M.; Orlando, R.; Mérawa, M.; Ugliengo, P. Cation Selectivity in Alkali-Exchanged Chabazite: An Ab Initio Periodic Study. *Chem. Mater.* **2003**, *15* (21), 3996–4004. <https://doi.org/10.1021/cm0342804>.
- (43) Nakatsuka, A. Dehydration Behavior of a Natural Hydrated Ca-Chabazite Studied by in-Situ High-Temperature Single-Crystal X-Ray Diffraction. *Microporous and Mesoporous Materials* **2021**, *11*.
- (44) Shang, J.; Li, G.; Singh, R.; Xiao, P.; Liu, J. Z.; Webley, P. A. Potassium Chabazite: A Potential Nanocontainer for Gas Encapsulation. *J. Phys. Chem. C* **2010**, *114* (50), 22025–22031. <https://doi.org/10.1021/jp107456w>.
- (45) Kresse, G.; Hafner, J. Ab Initio Molecular Dynamics for Liquid Metals. *Phys. Rev. B* **1993**, *47* (1), 558–561. <https://doi.org/10.1103/PhysRevB.47.558>.

- (46) Kresse, G.; Hafner, J. Ab Initio Molecular-Dynamics Simulation of the Liquid-Metal–Amorphous-Semiconductor Transition in Germanium. *Phys. Rev. B* **1994**, *49* (20), 14251–14269. <https://doi.org/10.1103/PhysRevB.49.14251>.
- (47) Kresse, G.; Furthmüller, J. Efficient Iterative Schemes for Ab Initio Total-Energy Calculations Using a Plane-Wave Basis Set. *Phys. Rev. B* **1996**, *54* (16), 11169–11186. <https://doi.org/10.1103/PhysRevB.54.11169>.
- (48) Perdew, J. P.; Burke, K.; Ernzerhof, M. Generalized Gradient Approximation Made Simple. *Phys. Rev. Lett.* **1996**, *77* (18), 3865–3868. <https://doi.org/10.1103/PhysRevLett.77.3865>.
- (49) Kohn, W.; Sham, L. J. Self-Consistent Equations Including Exchange and Correlation Effects. *Phys. Rev.* **1965**, *140* (4A), A1133–A1138. <https://doi.org/10.1103/PhysRev.140.A1133>.
- (50) Blöchl, P. E. Projector Augmented-Wave Method. *Phys. Rev. B* **1994**, *50* (24), 17953–17979. <https://doi.org/10.1103/PhysRevB.50.17953>.
- (51) Kresse, G.; Joubert, D. From Ultrasoft Pseudopotentials to the Projector Augmented-Wave Method. *Phys. Rev. B* **1999**, *59* (3), 1758–1775. <https://doi.org/10.1103/PhysRevB.59.1758>.
- (52) Tkatchenko, A.; Scheffler, M. Accurate Molecular van Der Waals Interactions from Ground-State Electron Density and Free-Atom Reference Data. *Phys. Rev. Lett.* **2009**, *102* (7), 073005. <https://doi.org/10.1103/PhysRevLett.102.073005>.
- (53) Bučko, T.; Lebègue, S.; Hafner, J.; Ángyán, J. G. Improved Density Dependent Correction for the Description of London Dispersion Forces. *J. Chem. Theory Comput.* **2013**, *9* (10), 4293–4299. <https://doi.org/10.1021/ct400694h>.
- (54) Bučko, T.; Lebègue, S.; Hafner, J.; Ángyán, J. G. Tkatchenko-Scheffler van Der Waals Correction Method with and without Self-Consistent Screening Applied to Solids. *Phys. Rev. B* **2013**, *87* (6), 064110. <https://doi.org/10.1103/PhysRevB.87.064110>.
- (55) Li, Z.; Huang, J.; Ye, L.; Lv, Y.; Zhou, Z.; Shen, Y.; He, Y.; Jiang, L. Encapsulation of Highly Volatile Fragrances in Y Zeolites for Sustained Release: Experimental and Theoretical Studies. *ACS Omega* **2020**, *5* (49), 31925–31935. <https://doi.org/10.1021/acsomega.0c04822>.
- (56) Himmetoglu, B.; Floris, A.; de Gironcoli, S.; Cococcioni, M. Hubbard-Corrected DFT Energy Functionals: The LDA+U Description of Correlated Systems. *International Journal of Quantum Chemistry* **2014**, *114* (1), 14–49. <https://doi.org/10.1002/qua.24521>.
- (57) Wang, L.; Maxisch, T.; Ceder, G. Oxidation Energies of Transition Metal Oxides within the GGA+U Framework. *Phys. Rev. B* **2006**, *73* (19), 195107. <https://doi.org/10.1103/PhysRevB.73.195107>.
- (58) Göttl, F.; Hafner, J. Structure and Properties of Metal-Exchanged Zeolites Studied Using Gradient-Corrected and Hybrid Functionals. I. Structure and Energetics. *The Journal of Chemical Physics* **2012**, *136* (6), 064501. <https://doi.org/10.1063/1.3676408>.
- (59) Grimme, S. Semiempirical GGA-Type Density Functional Constructed with a Long-Range Dispersion Correction. *J. Comput. Chem.* **2006**, *27* (15), 1787–1799. <https://doi.org/10.1002/jcc.20495>.
- (60) Göttl, F.; Grüneis, A.; Bučko, T.; Hafner, J. Van Der Waals Interactions between Hydrocarbon Molecules and Zeolites: Periodic Calculations at Different Levels of Theory, from Density Functional Theory to the Random Phase Approximation and Møller-Plesset Perturbation Theory. *The Journal of Chemical Physics* **2012**, *137* (11), 114111. <https://doi.org/10.1063/1.4750979>.
- (61) Andersen, H. C. Molecular Dynamics Simulations at Constant Pressure and/or Temperature. *The Journal of Chemical Physics* **1980**, *72* (4), 2384–2393. <https://doi.org/10.1063/1.439486>.

- (62) Frenkel, D.; Smit, B. *Understanding Molecular Simulation*; Computational science series; Academic Press, 2002.
- (63) Benco, L.; Bucko, T.; Hafner, J.; Toulhoat, H. Periodic DFT Calculations of the Stability of Al/Si Substitutions and Extraframework Zn²⁺ Cations in Mordenite and Reaction Pathway for the Dissociation of H₂ and CH₄. *J. Phys. Chem. B* **2005**, *109* (43), 20361–20369. <https://doi.org/10.1021/jp0530597>.
- (64) Görtl, F.; Buló, R. E.; Hafner, J.; Sautet, P. What Makes Copper-Exchanged SSZ-13 Zeolite Efficient at Cleaning Car Exhaust Gases? *J. Phys. Chem. Lett.* **2013**, *4* (14), 2244–2249. <https://doi.org/10.1021/jz400817c>.
- (65) Hessou, E. P.; Jabraoui, H.; Khalil, I.; Dziurla, M.-A.; Badawi, M. Ab Initio Screening of Zeolite Y Formulations for Efficient Adsorption of Thiophene in Presence of Benzene. *Applied Surface Science* **2021**, *541*, 148515. <https://doi.org/10.1016/j.apsusc.2020.148515>.
- (66) Dědeček, J.; Sobalík, Z.; Wichterlová, B. Siting and Distribution of Framework Aluminium Atoms in Silicon-Rich Zeolites and Impact on Catalysis. *Catalysis Reviews* **2012**, *54* (2), 135–223. <https://doi.org/10.1080/01614940.2012.632662>.
- (67) Frising, T.; Leflaive, P. Extraframework Cation Distributions in X and Y Faujasite Zeolites: A Review. *Microporous and Mesoporous Materials* **2008**, *114* (1–3), 27–63. <https://doi.org/10.1016/j.micromeso.2007.12.024>.
- (68) Losch, P.; Joshi, H. R.; Vozniuk, O.; Grünert, A.; Ochoa-Hernández, C.; Jabraoui, H.; Badawi, M.; Schmidt, W. Proton Mobility, Intrinsic Acid Strength, and Acid Site Location in Zeolites Revealed by Varying Temperature Infrared Spectroscopy and Density Functional Theory Studies. *J. Am. Chem. Soc.* **2018**, *140* (50), 17790–17799. <https://doi.org/10.1021/jacs.8b11588>.
- (69) Ridha, F. N.; Webley, P. A. Anomalous Henry's Law Behavior of Nitrogen and Carbon Dioxide Adsorption on Alkali-Exchanged Chabazite Zeolites. *Separation and Purification Technology* **2009**, *67* (3), 336–343. <https://doi.org/10.1016/j.seppur.2009.03.045>.
- (70) Khelifa, A.; Derriche, Z.; Bengueddach, A. Sorption of Carbon Dioxide by Zeolite X Exchanged with Zn²⁺ and Cu²⁺. *Microporous and Mesoporous Materials* **1999**, *32* (1–2), 199–209. [https://doi.org/10.1016/S1387-1811\(99\)00107-9](https://doi.org/10.1016/S1387-1811(99)00107-9).
- (71) Jacobs, W. P. J. H.; van Wolput, J. H. M. C.; van Santen, R. A. An in Situ Fourier Transform Infrared Study of Zeolitic Vibrations: Dehydration, Deammoniation, and Reammoniation of Ion-Exchanged Y Zeolites. *Zeolites* **1993**, *13* (3), 170–182. [https://doi.org/10.1016/S0144-2449\(05\)80274-X](https://doi.org/10.1016/S0144-2449(05)80274-X).
- (72) Loewenstein, W. The Distribution of Aluminum in the Tetrahedra of Silicates and Aluminates. *Am. Mineral.* **1954**, *39* (1–2), 92–96.
- (73) Mlekodaj, K.; Dedecek, J.; Pashkova, V.; Tabor, E.; Klein, P.; Urbanova, M.; Karcz, R.; Sazama, P.; Whittleton, S. R.; Thomas, H. M.; Fishchuk, A. V.; Sklenak, S. Al Organization in the SSZ-13 Zeolite. Al Distribution and Extraframework Sites of Divalent Cations. *J. Phys. Chem. C* **2019**, *123* (13), 7968–7987. <https://doi.org/10.1021/acs.jpcc.8b07343>.
- (74) Hun Kwak, J.; Zhu, H.; Lee, J. H.; Peden, C. H. F.; Szanyi, J. Two Different Cationic Positions in Cu-SSZ-13? *Chem. Commun.* **2012**, *48* (39), 4758. <https://doi.org/10.1039/c2cc31184d>.
- (75) Andersen, C. W.; Bremholm, M.; Vennestrøm, P. N. R.; Blichfeld, A. B.; Lundegaard, L. F.; Iversen, B. B. Location of Cu²⁺ in CHA Zeolite Investigated by X-Ray Diffraction Using the Rietveld/Maximum Entropy Method. *IUCrJ* **2014**, *1* (6), 382–386. <https://doi.org/10.1107/S2052252514020181>.

- (76) Chibani, S.; Chebbi, M.; Lebègue, S.; Bučko, T.; Badawi, M. A DFT Investigation of the Adsorption of Iodine Compounds and Water in H-, Na-, Ag-, and Cu- Mordenite. *The Journal of Chemical Physics* **2016**, *144* (24), 244705. <https://doi.org/10.1063/1.4954659>.
- (77) Sangthong, W.; Sirijaraensre, J. Understanding the Effect of the Divalent Cations (Ni, Cu, and Zn) Exchanged FAU Zeolite on the Kinetic of CO₂ Cycloaddition with Ethylene Oxide: A DFT Study. *Journal of Molecular Graphics and Modelling* **2022**, *117*, 108321. <https://doi.org/10.1016/j.jmgm.2022.108321>.
- (78) Li, X.; Shen, W.; Sun, H.; Meng, L.; Wang, B.; Zhan, C.; Zhao, B. Theoretical Studies on Carbon Dioxide Adsorption in Cation-Exchanged Molecular Sieves. *RSC Adv.* **2020**, *10* (53), 32241–32248. <https://doi.org/10.1039/D0RA05228K>.
- (79) Mikosch, H.; Uzunova, E. L.; St. Nikolov, G. Interaction of Molecular Nitrogen and Oxygen with Extraframework Cations in Zeolites with Double Six-Membered Rings of Oxygen-Bridged Silicon and Aluminum Atoms: A DFT Study. *J. Phys. Chem. B* **2005**, *109* (22), 11119–11125. <https://doi.org/10.1021/jp0451795>.
- (80) Gopalsamy, K.; Wahiduzzaman, M.; Daouli, A.; Badawi, M.; Maurin, G. Computational Exploration of a Metal(II) Catecholate-Functionalized UiO-66 Nanoporous Metal–Organic Framework for Effective NO_x Capture. *ACS Appl. Nano Mater.* **2022**. <https://doi.org/10.1021/acsnm.2c03284>.
- (81) Barbosa, L. A. M. M.; van Santen, R. A. The Activation of H₂ by Zeolitic Zn(II) Cations. *J. Phys. Chem. C* **2007**, *111* (23), 8337–8348. <https://doi.org/10.1021/jp070677+>.
- (82) Areán, C. O.; Palomino, G. T.; Carayol, M. R. L.; Pulido, A.; Rubeš, M.; Bludský, O.; Nachtigall, P. Hydrogen Adsorption on the Zeolite Ca-A: DFT and FT-IR Investigation. *Chemical Physics Letters* **2009**, *477* (1–3), 139–143. <https://doi.org/10.1016/j.cplett.2009.06.058>.
- (83) García, E. J.; Pérez-Pellitero, J.; Pirngruber, G. D.; Jallut, C.; Palomino, M.; Rey, F.; Valencia, S. Tuning the Adsorption Properties of Zeolites as Adsorbents for CO₂ Separation: Best Compromise between the Working Capacity and Selectivity. *Ind. Eng. Chem. Res.* **2014**, *53* (23), 9860–9874. <https://doi.org/10.1021/ie500207s>.